Powder Technology 323 (2018) 284–293

Contents lists available at ScienceDirect

Powder Technology

journal homepage: www.elsevier.com/locate/powtec

Numerical investigation of particle deposition in a triple bifurcation airway due to gravitational sedimentation and inertial impaction

Xiaole Chen [a], Yu Feng [b], Wenqi Zhong [a,*], Baobin Sun [c], Feng Tao [c]

[a] Key Laboratory of Energy Thermal Conversion and Control of Ministry of Education, Southeast University, Nanjing, Jiangsu Prov. 210096, China
[b] School of Chemical Engineering, Oklahoma State University, Stillwater, OK 74078, USA
[c] School of Medicine, Southeast University, Nanjing, Jiangsu Prov. 210096, China

ARTICLE INFO

Article history:
Received 21 July 2017
Received in revised form 19 September 2017
Accepted 24 September 2017
Available online 4 October 2017

Keywords:
Inhalable particle
Gravitational sedimentation
Inertial impaction
Deposition efficiency
Airway

ABSTRACT

Focusing on the particle deposition due to gravitational sedimentation and inertial impaction, the transport and deposition of micron particles with various diameters (i.e., 1 to 7 μm) have been simulated in a triple bifurcation airway at flow rates of 15 to 120 L/min. The airway configurations for generation 11 to generation 14 are determined by matching the Stokes number *St* and the sedimentation parameter γ (Particuology, 2016, 28:102–113). Air flow distributions, local deposition patterns, and deposition efficiencies are compared between simulations with and without gravity. The results suggest that minimum deposition efficiency exists for large particles indicating the change of dominant deposition mechanism between sedimentation and impaction. Sedimentation governed particle deposition is also observed for small particles. A revised correlation for predicting DE as a function of Stokes number and sedimentation parameter is proposed for $5.78 \times 10^{-4} < St < 0.226$ and $1.54 \times 10^{-4} < \gamma < 0.06$. These findings could be utilized to design the drug particle property and inhalation waveform for the high-efficiency pulmonary drug delivery.

1. Introduction

In light of advancing manufacture methods for pharmaceutical particles, pulmonary drug delivery now attracts increasing attentions [1]. To enhance the drug delivery efficiency to local lesions in the lung, it is critical to understand the particle transport dynamics and deposition mechanism in human airways.

For inhaled particulate matters, primary deposition mechanisms include inertial impaction [2–4], gravitational sedimentation [5,6], as well as Brownian motion. Brownian motion mainly affects submicron particles [7–9]. In contrast, for micron particles, inertial impaction governs the deposition in the upper airway, while sedimentation plays the dominant role in the alveolar region. Compared to the many research investigating the different parameters that affect the two different deposition mechanisms [10–27], there are limited investigations regarding the transition of the dominant deposition mechanism [5,28–31]. Specifically, for a given particle diameter and inhalation flow rate, the key question remains unanswered, e.g., is it possible to find an airway generation in which inertial impaction and sedimentation provide a similar contribution to the particle deposition (see Fig. 1)? Such investigations will contribute to the discovery of the airway region with minimum deposition efficiency (DE) associated with specific particle properties and breathing patterns. Therefore, studying the contributions of different deposition mechanisms could be utilized for optimization of drug formulation and pulmonary drug delivery operations. For example, drug particle properties and breathing pattern could be designed on a patient-specific level, to match these conditions with the lowest regional DEs in the transition regions, thereby guarantee a higher drug delivery efficiency in the alveolar region for a better translocation performance into systemic regions via blood circulation [32]. Another potential application example is the pulmonary targeted drug delivery to treat localized lung tumor [33] or diseased areas [34] in the transition regions by controlling the operational parameters for drug inhalation, such as inhalation flow rate and breath holding duration. In such a method, the local deposition will be increased by the enhanced sedimentation effect.

Hofmann et al. simulated the simulated the transport of 10 μm particles from G15 ("G" stands for generation) to G16 with gravity [35]. Ma et al. [36] compared the cross-sectional velocity contours and particle trajectories between CFD simulations and experimental results in a scaled-up alveolated airway model. The comparison indicates that CFD techniques can provide an accurate prediction for air flow and particle transport in alveoli. Furthermore, Ma and Darquenne studied the depositions of 1 μm and 3 μm particles in models of the human alveolar sac and terminal acinar bifurcation under rhythmic wall motion for two breathing conditions [37]. Sznitman et al. investigated the transport and deposition of 1 μm and 3 μm particles in two acinar models, i.e., a

* Corresponding author.
E-mail address: wqzhong@seu.edu.cn (W. Zhong).

https://doi.org/10.1016/j.powtec.2017.09.050
0032-5910/

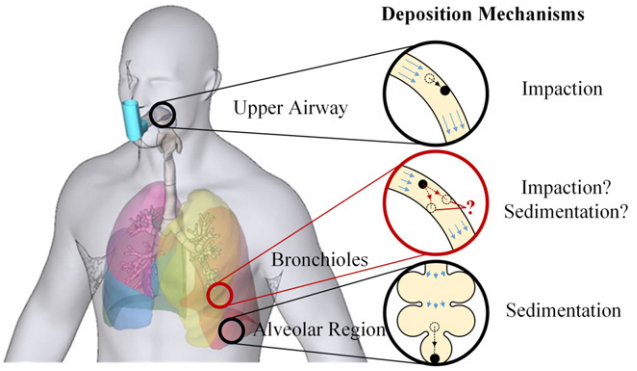

Fig. 1. Schematics of particle deposition mechanisms in human airway.

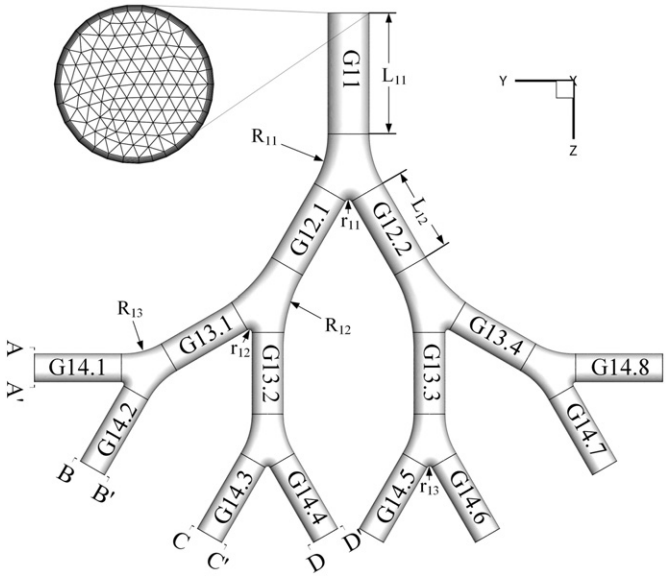

Fig. 2. Schematics of the G11 to G14 airway model and mesh.

simple alveolar duct and a space-filling acinar branching tree, with sinusoidal breathing waveform [30]. The results suggested that the dominant deposition mechanism changes from convection to sedimentation within a span of 2 μm. Piglione et al. concluded that Froude number is the key parameter to determine the relative importance of impaction and settling [38]. However, *Fr* does not include the length parameters of the airway, i.e., length and diameter of the airway duct. Kleinstreuer et al. proposed the non-dimensional sedimentation parameter γ to indicate the significance of sedimentation when simulating the particle transport and deposition in a G6–G9 airway model [5]. Their results claimed that gravitational deposition might become dominant for large particles (>5 μm) at a flow rate of 3.75 L/min. Our previous experimental measurements of the deposition of fibers indicated that the deposition fraction (DF) increases linearly with the increasing γ when the fibers are relatively large [39]. Additionally, a

Table 1
Geometric parameters for the G11–G14 airway model.

Airway generation	Geometrical size(mm)			
	Diameter, D_i	Length, L_i	Lateral radius, R_i	Inner radius, r_i
G11	1.09	3.213	2.565	0.095
G12	0.95	2.268	3.854	0.082
G13	0.82	2.165	1.998	0.074
G14	0.74	2.300	–	–

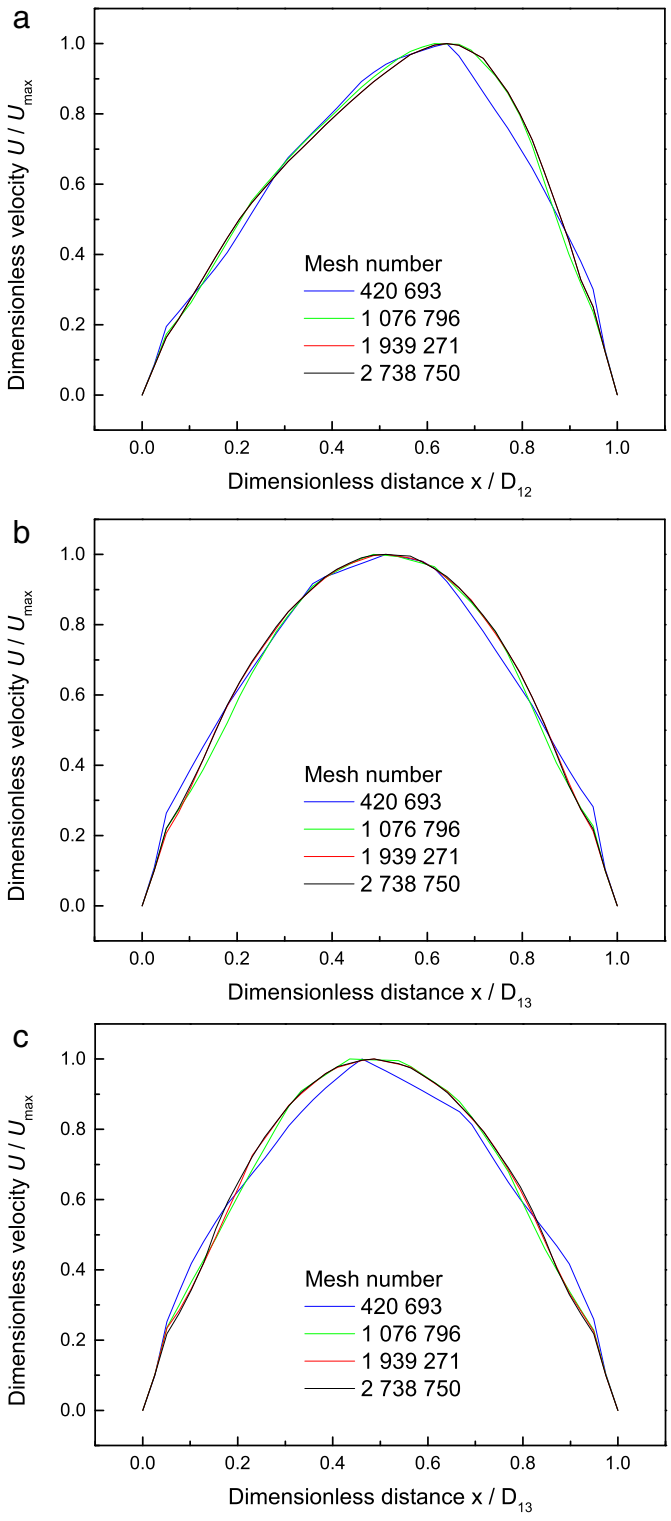

Fig. 3. Comparisons of velocity profiles in different generations for mesh independence test: (a) G12; (b) G13.1; (c) G14.1.

method matching Stokes number *St* and sedimentation parameter γ were proposed to correlate similar deposition characteristics in the lower airway with the experiment results. Still, existing papers do not provide systematic investigations and conclusions on the relationship between dominant deposition mechanism types and different airway generations.

To fill the knowledge gap and provide an insightful discussion, this paper focuses on simulating the particle deposition due to

Table 2
Stokes numbers for particles with different diameters under different flow rate conditions.

Flow rate (L/min)	Reynolds number	Particle diameter (μm)						
		1	2	2.5	3	4	5	7
15	9.76	5.78E−4	2.31E−3	3.61E−3	5.20E−3	9.24E−3	1.44E−2	2.83E−2
30	19.52	1.16E−3	4.62E−3	7.22E−3	1.04E−2	1.85E−2	2.89E−2	5.66E−2
45	29.28	1.73E−3	6.93E−3	1.08E−2	1.56E−2	2.77E−2	4.33E−2	8.49E−2
60	39.05	2.31E−3	9.24E−3	1.44E−2	2.08E−2	3.70E−2	5.78E−2	1.13E−1
90	58.57	3.47E−3	1.39E−2	2.17E−2	3.12E−2	5.55E−2	8.66E−2	1.70E−1
120	78.09	4.62E−3	1.85E−2	2.89E−2	4.16E−2	7.39E−2	1.16E−1	2.26E−1

sedimentation and inertial impaction, the transport and deposition of micron particles with various diameters (i.e., 1 to 7 μm) in a G11–G14 airway at flow rates of 15 to 120 L/min using Computational Fluid-Particle Dynamics (CFPD) method. Extra simulations without gravity are also performed for comparison purposes. Airflow distributions, deposition patterns, and deposition efficiencies are compared. The minimum DEs are found for large particles, and gravitational sedimentation governed deposition is also observed for small particles. A revised correlation of DE prediction is proposed, which is a function of Stokes number and sedimentation parameter.

2. Triple bifurcation airway unit

To investigate the particle deposition as they travel into the deeper airways, it is essential to determine the critical generation where gravitational sedimentation becomes dominant compared to inertial impaction. Therefore, sedimentation parameter γ is introduced which is defined as [5]:

$$\gamma = \left(\frac{v_{settling}}{U}\right)\left(\frac{L}{D}\right)cos\varphi \tag{1}$$

where $v_{settling}$ is the particle settling velocity, U is the average air velocity, L is the length of the airway, D is the diameter of the airway, φ is the inclination angle measured relative to the horizontal. The sedimentation parameter includes two more length parameters of the airway, i.e., L and D, than the Froude number $Fr = U/\sqrt{gD}$. According to this advantage, Kleinstreuer et al. [5] suggested that γ is more suitable than Fr for the estimation of particle sedimentation in lower airways.

Our previous experiments indicated that the effect of the gravity on particle deposition could not be neglected when $0.0228 < \gamma < 0.247$ [39]. The results also suggested that the experimental data could be used to determine the appropriate inhalation patterns leading to the dominant sedimentation effect in a designated airway generation, by matching the Stokes number St and sedimentation parameter γ. Specifically, St is defined as

$$St = \frac{\rho_p d_p^2 U}{18\mu D} \tag{2}$$

where ρ_p is the particle density, d_p is the particle diameter and μ are the dynamic viscosity of air.

Specifically, once particle properties are known, and the airway generation is assigned, the average air velocity U, i.e., inhalation flow rate at the oral/nasal inlets, could be calculated from Eqs. (1) and (2) using γ and St obtained from experiments [39]. Note that it is possible that the calculated flow rate is not within the reasonable range (i.e., 15 to 120 L/min). However, for those generations with reasonable flow rates, the particle deposition would share similar characteristics as the experiments, i.e., governed by gravitational sedimentation.

Concluded by Chen et al. [39], the pulmonary generation G10 to G14 cover a relatively wide range of reasonable inhalation flow rates for both St and γ. Simulation results suggested that four generations of the pulmonary airway could accurately predict the effect of the air flow of the upper and lower generations on the particle deposition [40,41]. Therefore, a triple bifurcation airway model including G11 to G14 is chosen for the following analysis of the air flow distributions and particle depositions.

3. Methodology

3.1. Governing equations for airflow

For inhalation flow rate $15 < Q_{in} < 120$ L/min, The Reynolds number at the inlet of G11 ranges from 9.76 to 78.09 correspondingly. Thus, the airflow regime in the triple bifurcation airway model is laminar. Accordingly, the governing equations for the incompressible flow, i.e., the conservation of mass and momentum, can be given as:

$$\nabla\vec{u} = 0 \tag{3}$$

$$\left(\vec{u}\cdot\nabla\right)\vec{u} + \frac{\partial\vec{u}}{\partial t} = -\frac{\nabla p}{\rho} + \nabla\cdot\left[v\left(\nabla\vec{u} + (\nabla\vec{u})^{tr}\right)\right] \tag{4}$$

where $\vec{u}$ is the air velocity, t is time, p is the air pressure, ρ is the air density, and $(\nabla\vec{u})^{tr}$ is the transpose of $\nabla\vec{u}$.

3.2. Governing equations for particle transport

Assuming the particle suspension in the lower airways is dilute, the particle-particle interaction is neglected. Additionally, Brownian motion

Table 3
Sedimentation parameters for particles with different diameter under different flow rate conditions.

Flow rate (L/min)	Reynolds number	Particle diameter (μm)						
		1	2	2.5	3	4	5	7
15	9.76	1.23E−3	4.93E−3	7.70E−3	1.11E−2	1.97E−2	3.08E−2	6.04E−2
30	19.52	6.16E−4	2.47E−3	3.85E−3	5.55E−3	9.86E−3	1.54E−2	3.02E−2
45	29.28	4.11E−4	1.64E−3	2.57E−3	3.70E−3	6.57E−3	1.03E−2	2.01E−2
60	39.05	3.08E−4	1.23E−3	1.93E−3	2.77E−3	4.93E−3	7.70E−3	1.51E−2
90	58.57	2.05E−4	8.22E−4	1.28E-3	1.85E−3	3.29E−3	5.14E−3	1.01E−2
120	78.09	1.54E−4	6.16E−4	9.63E−4	1.39E−3	2.47E−3	3.85E−3	7.55E−3

effect is negligible. Thus, the effects of drag force and gravity are considered for predicting the particle trajectory, i.e.,

$$m_p \frac{\mathrm{d}\vec{u}_p}{\mathrm{d}t} = \vec{F}_D + m_p\left(\rho_p - \rho\right)\frac{\vec{g}}{\rho_p} \tag{5}$$

where $\vec{F}_D$ is the drag force, which is defined as

$$\vec{F}_D = \frac{1}{8}\pi d_p^2 C_D\left(\vec{u} - \vec{u}_p\right)\left|\vec{u} - \vec{u}_p\right| \tag{6}$$

where C_D is the drag coefficient, which is given as [42]:

$$C_D = \frac{a_1}{\mathrm{Re}_p} + \frac{a_2}{\mathrm{Re}_p^2} + a_3 \tag{7}$$

where a_1, a_2, and a_3 are coefficients. The particle Reynolds number is defined as

$$\mathrm{Re}_p = \frac{\rho \mid \vec{u} - \vec{u}_p \mid d_p}{\mu} \tag{8}$$

3.3. Geometry and mesh

Due to the limitation of the current technology, it is still difficult to obtain the realistic airway model directly from the CT or MRI scan. Thus, a triple bifurcation airway unit from G11 to G14 was constructed based on Weibel's 23-generation pulmonary model [43] (see Fig. 2). The bifurcation angle for each generation is 60°. Inner and lateral curves with different diameters were used to generate smooth connections

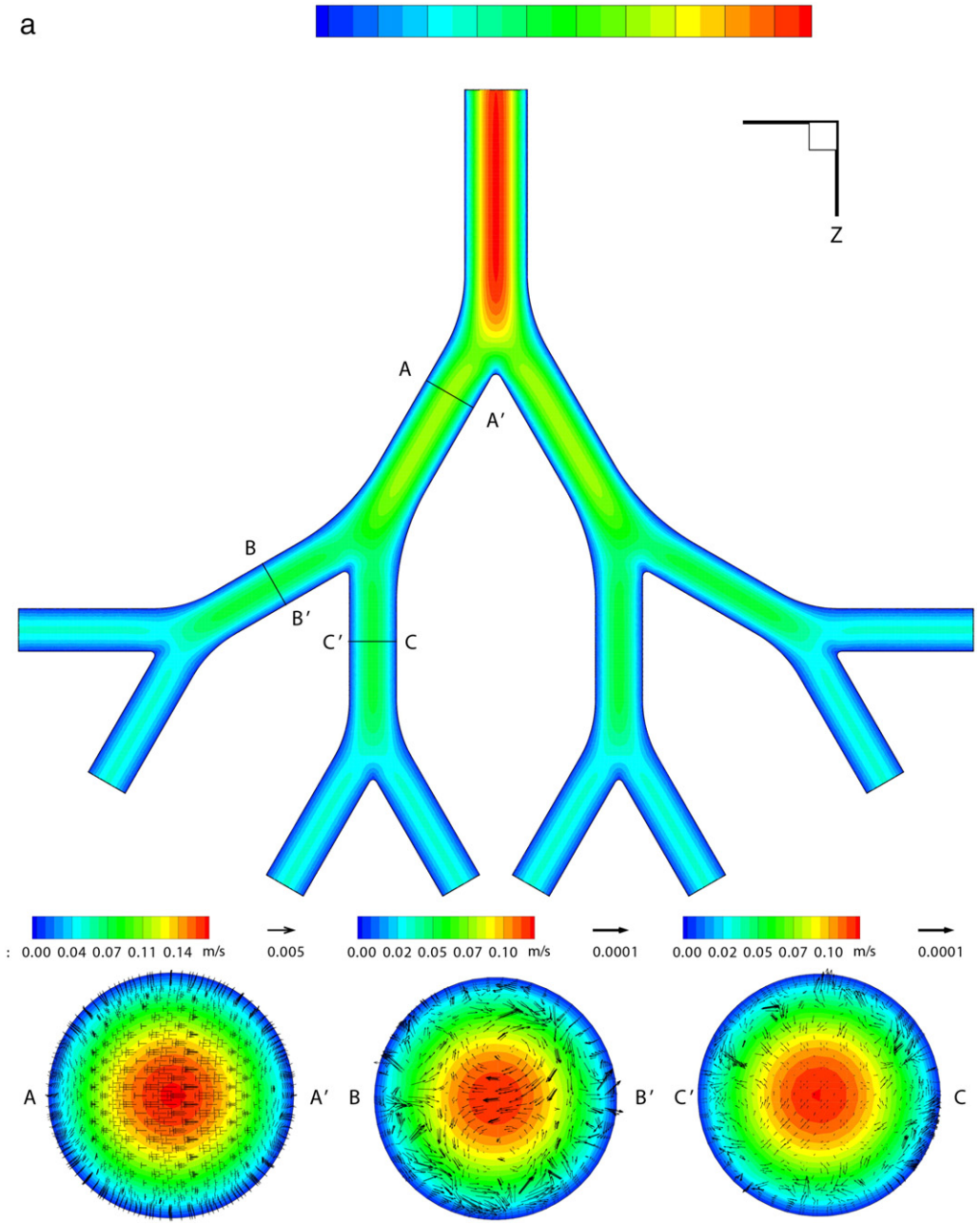

Fig. 4. Airflow distributions in the triple bifurcation airway at different flow rates: (a) 15 L/min; (b) 60 L/min; (c) 120 L/min.

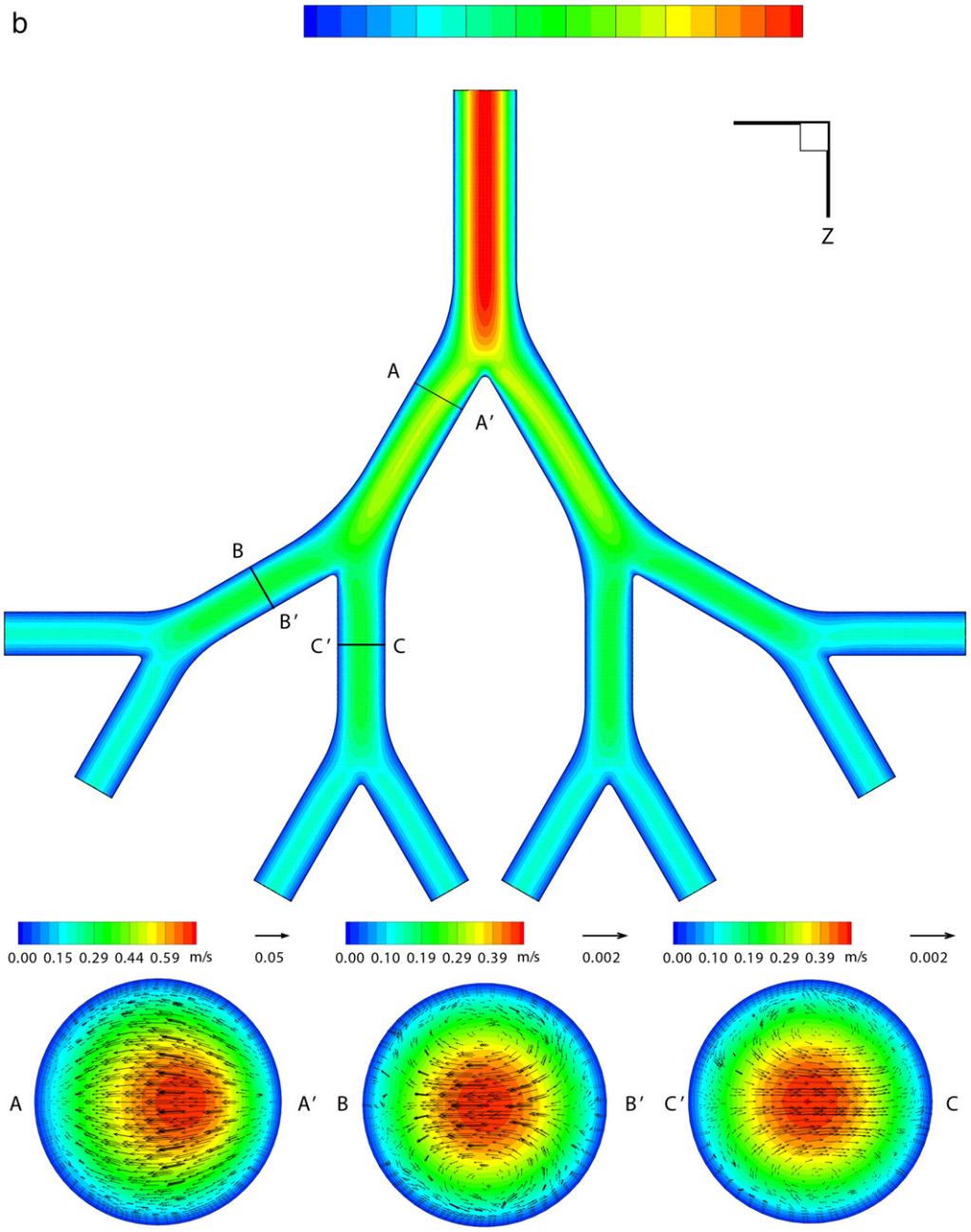

Fig. 4 (*continued*).

between airway generations. The details of the geometric parameters are summarized in Table 1.

Tetrahedral mesh with prism layers was generated for the numerical simulation. To obtain an airflow independent of the mesh number, four meshes with different mesh number, i.e., 420,693, 1,076,796, 1,939,271 and 2,738,750, were generated for the mesh independence test. The dimensionless velocity profiles of the mid-plane in G12, G13.1, and G13.2 were compared at the flow rate of 120 L/min (see Fig. 3). Note that the average velocity at the inlet of G11 is calculated based on the assumption that each airway generation would have two daughter tubes. Thus, the actual volume flow rate in G11 is $120/2^{11}$ L/min, i.e., 0.0586 L/min, if the inhalation flow rate is 120 L/min at the oral/nasal inlet. Considering the differences of dimensionless velocity profiles between the 1.93 million and 2.73 million meshes in Fig. 3 are all smaller than 5%, the mesh with 1.93 mesh cells was used as the final mesh for this study.

3.4. Numerical setup

In light of the dilute particle suspension, one-way coupling was applied in the simulations. The airflow distributions were solved first for different inhalation flow rates at the inlet of oral/nasal cavity, i.e., 15, 30, 45, 60, 90 and 120 L/min. User defined function (UDF) was used to generate the parabolic velocity inlet for each case [44]. The simulation for the airflow was considered converged when the residual became $<10^{-5}$.

To obtain the correlation between particle deposition efficiency and Stokes number in a relatively wide range, the simulations of particle

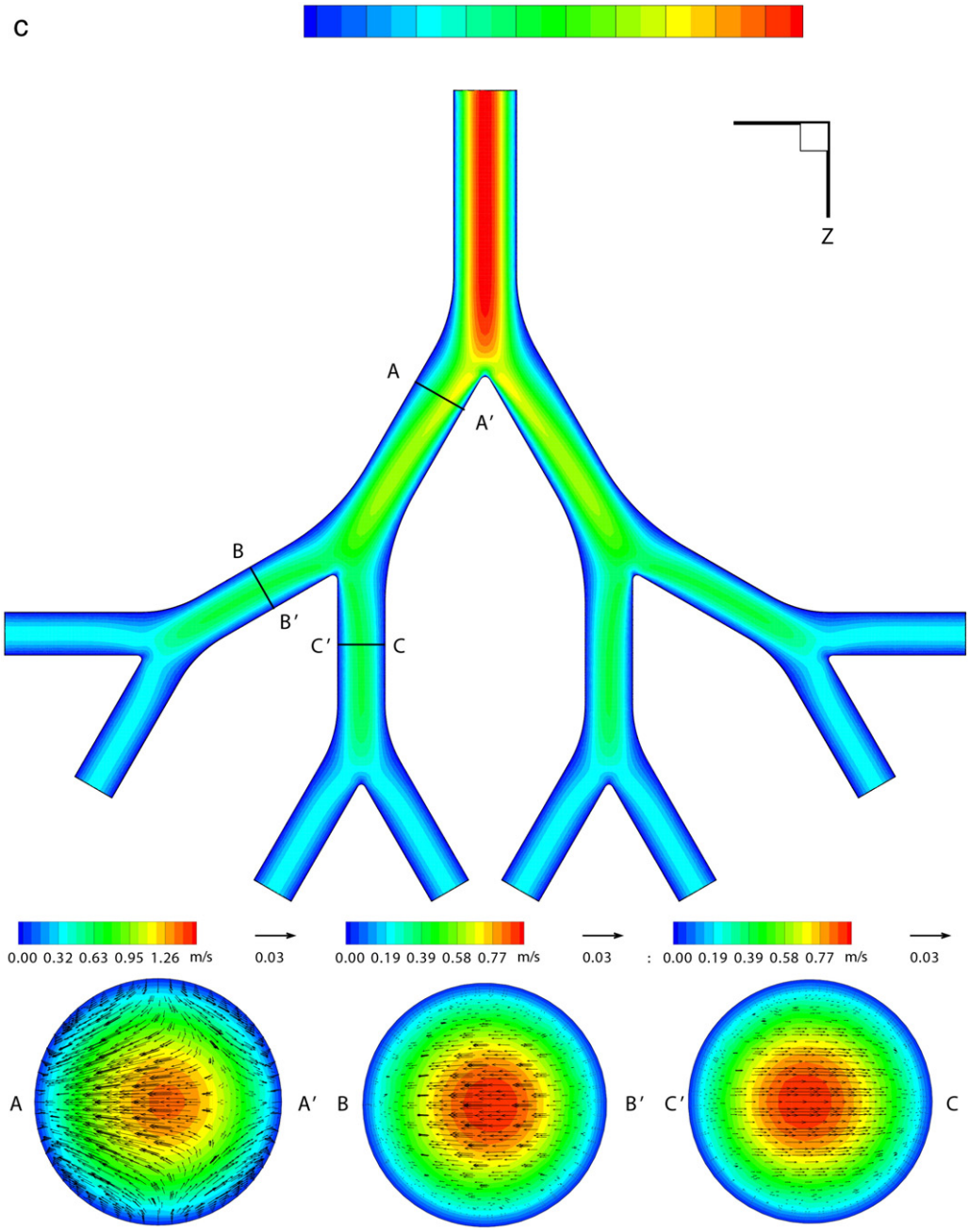

Fig. 4 (*continued*).

transport and deposition were carried out for particles with a density of 1550 kg/m^3 and diameters from 1 to 7 μm. An in-house C++ code was generated to determine the initial position of the particle at the inlet of G11. It generates a random distribution with a parabolic probability density which is proportional to the air velocity. The particle is assumed to have the same velocity as the local air at the inlet. For each case, 50,000 particles were generated, and their trajectories were calculated respectively. Particle deposition was assumed to occur when the particle contacted with the airway boundary. The locations of deposited and escaped particles were exported via another UDF when the deposition or the escape happened. The Stokes numbers and sedimentation parameters for the different cases used in this study are presented in Table 2 and Table 3, respectively. The gravity direction was vertical to the mid-plane towards the –x direction as shown in Fig. 2. An extra set of simulations without gravity were also performed to disseminate the deposition caused by inertial impaction from gravitational sedimentation.

Table 4
Flow distributions at the outlets under different flow rate conditions.

Inhalation flow rate (L/s)	Ratio (%)			
	G14.1	G14.2	G14.3	G14.4
15	12.5090	12.4889	12.5036	12.4986
60	12.5064	12.4911	12.5046	12.4979
120	12.5088	12.4975	12.4999	12.4939

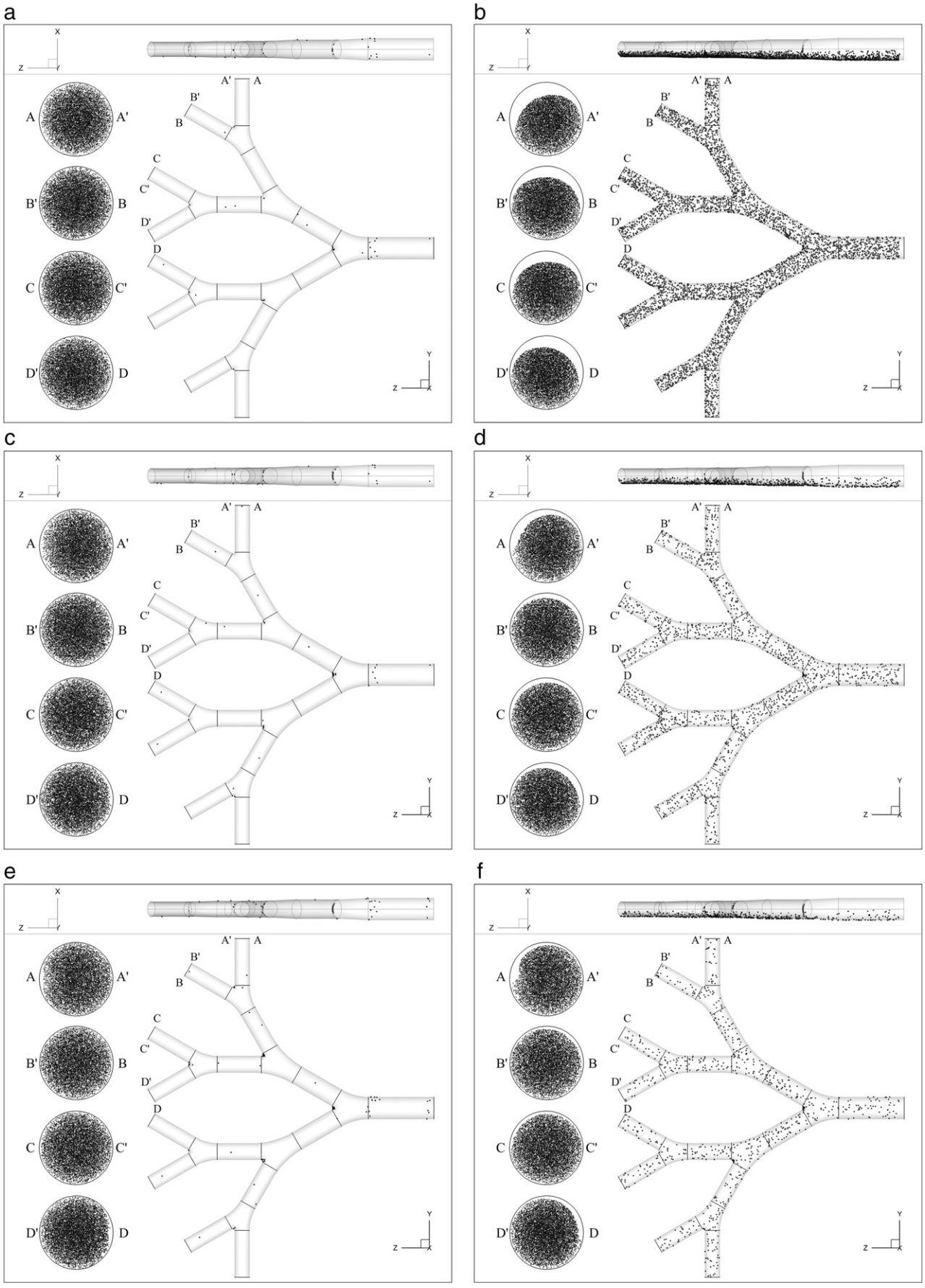

Fig. 5. Comparison of deposition patterns and locations of escaped particles between simulations with and without gravity: (a) 15 L/min, without gravity; (b) 15 L/min, with gravity; (c) 60 L/min, without gravity; (d) 60 L/min, with gravity; (e) 120 L/min, without gravity; (f) 120 L/min, with gravity.

4. Results and discussion

4.1. Airflow distributions

Fig. 4 illustrates the air velocity contours of the mid-plane and the cross-sectional velocity contours and secondary flow vectors at the flow rate of 15, 60 and 120 L/min. The reference vectors are adjusted to present the secondary flows. It is evident that the velocity distributions of the air in Fig. 4 show the distinct difference from that of the upper lung generations. The simulations in the G3–G6 airway by Zhang et al. showed that the velocity profiles in the daughter tubes were skewed indicating strong secondary flows, e.g., the maximum secondary velocity could reach 21% of the mean inlet velocity [45]. In contrast, the spatial positions of the highest velocity in the cross sections (i.e., the E-E′, F-F′ and G′-G cross sections are shown in Fig. 4) located in the center of the airway tubes in this study. Thus, the secondary flow is relatively weak, i.e., 2 to 3 magnitudes smaller than maximum velocity in the cross section. The flow distributions at the outlets (i.e., G14.1 to G14.2) are almost ideally even (see Table 4).

4.2. Final particle distributions

The final distributions of the 2.5 μm particles, i.e., the locations of deposited and escaped particles, are shown in Fig. 5 for the inhalation flow rates of 15, 60 and 120 L/min conditions with and without gravity. Considering the airway model is symmetric about plane $y = 0$, positions of the escaped particles at the G14.5 to G14.8 outlets are mirrored to G14.4 to G14.1 outlets shown in Fig. 5.

For the simulation cases without gravity, the main deposition mechanism would be inertial impaction. As shown in Figs. 5 (a), (c) and (e), this type of deposition enhances with the increase of flow rate. Despite few scattered deposition on the airway tubes due to the secondary flow, most deposition occurred in the bifurcation regions. It is interesting to find that the distributions of escaped particles at the outlets are similar to the parabolic-shaped probability density distribution when releasing the particles at the inlet of G11.

When the effect of the gravity on the particle is considered in the simulations, the deposition patterns (see Figs. 5(b), (d) and (f)) show a significant difference compared to the ones without gravity. Almost all particle deposition occurred on the boundary of the bottom half of the airway except the depositions near the bifurcating regions. This indicates that gravitational sedimentation is the dominant deposition mechanism. This significant difference is caused by the slow airflow in the G11 to G14 airway. When the effect of the gravity is not included, the velocities of the particles are relatively small due to the slow airflow, and therefore, most particles can well follow the airflow in the bifurcating region instead of colliding onto the airway boundary. In contrast, the particles gradually settle down and deposit on the bottom of the airway when gravity is considered. It is also worth noting that the number of deposited particles reduces with increased flow rate, which suggests that the particles are entrained to the subsequent airways instead of depositing on the bottom of the airway. There are crescent areas free of particles at the four outlets. This indicates that the particles move towards the direction of the gravity while the secondary flow is too weak to bring the particle upward due to Dean's flow.

4.3. Deposition efficiencies

4.3.1. DE vs. St

The particle deposition efficiencies obtained from the simulations with and without gravity are plotted against the Stokes number as shown in Fig. 6. The DEs for simulations under 6 different flow rate conditions without gravity, which are shown as black dots, are concentrated. These data fit the correlation proposed by Kim and Fisher [10], i.e., $DE = (1 - 1/(C_1 St^{C_2} + 1)) \times 100\%$, very well (see the black dash line in Fig. 6). If $C_1 = 14.76$ and $C_2 = 2.34$, for variance analysis, the adjusted R^2 value would be 0.989.

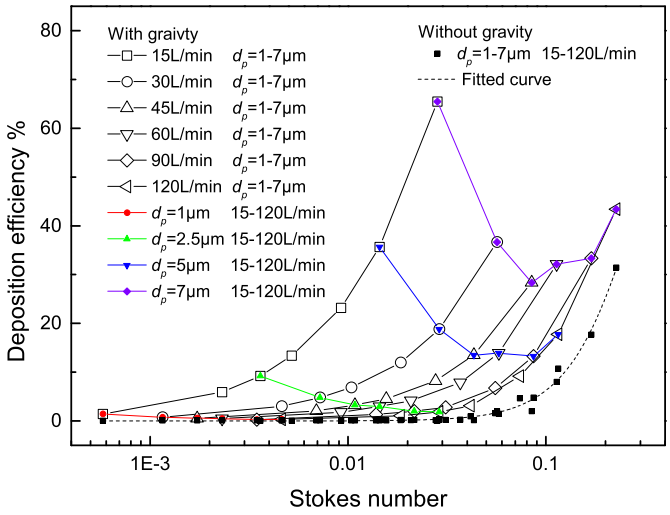

Fig. 6. DE vs. *St* for simulations in the triple bifurcation airway with and without gravity.

However, the DEs for simulations with gravity are more scattered in Fig. 6. Thus, these data points are organized by two individual parameters, i.e., the same flow rate and the same particle diameter. For the same flow rate (solid black lines in Fig. 6), the DEs all increase with the growth of *St*. The increasing trend is similar to Kim and Fisher's correlation [10]. Still, the DEs under different inhalation flow rate conditions have significant divergence for the same *St*. It suggests that there is an extra factor, gravity, in this case, affecting the DE.

For the same particle diameter (solid colorful lines in Fig. 6), the particle deposition behaviors are different from the results of the upper airway. It is well known that the DEs increase with higher flow rate from the oral [46] or nasal cavity [47,48] to the upper lung generations [4, 49]. The DE-curves of 1 μm and 2.5 μm decrease with the increase of *St*. This is in contradiction to the traditional suggestion for pulmonary drug delivery, which encourages slow inhalation for drug administration. Thus, a careful design of the inhalation waveform might be considered for the inhalable drug delivery aiming the deeper lung regions. Meanwhile, the curves of 5 μm and 7 μm decrease first, reach the lowest DE points, and then increase with *St* again. It proves the assumption that when the effect of gravity on the particle deposition increases and air velocity gradually decreases towards the lower airway generations, a minimum DE point exists. Therefore, the DE cannot be correlated by *St* alone, and the effect of gravity should be included.

4.3.2. DE vs. γ

In the previous experiment, the DE increases linearly with the increase of γ under low inhalation flow rate conditions [39]. For the same flow rate, the DE does increase linearly with increasing γ (see Fig. 7(a)). However, slopes still vary between different flow rates.

Assuming that the depositions caused by inertial impaction and sedimentation are independent to each other, the DE caused by sedimentation could be obtained by subtracting the DE of the simulations without gravity from the DE of simulations with gravity. Fig. 7(b) plots these DEs from the direct subtraction against γ. The linear correlation for these DEs excluding inertial impaction is relatively accurate. However, the DEs under the flow rate conditions in the middle range, i.e., 45 and 60 L/min, still have minor deviations from the linear correlation, which suggests that the depositions caused by inertial impaction and sedimentation are related.

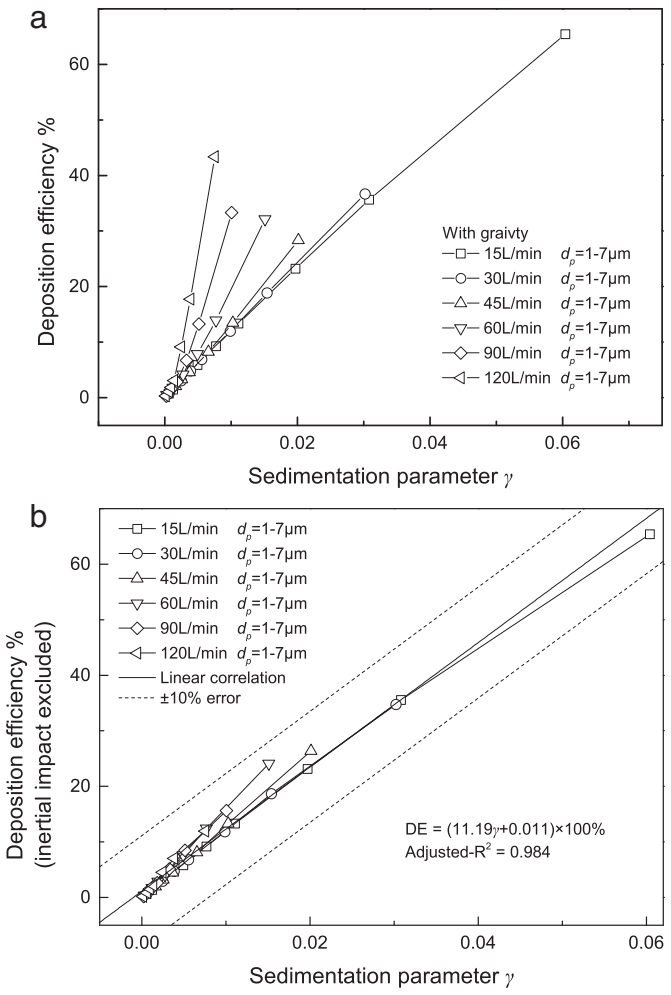

Fig. 7. DE vs. γ for simulations in the triple bifurcation airway with gravity: (a) DE vs. γ; (b) DE excluding inertial impaction vs. γ, and linear correlation.

4.3.3. Correlation for DE

Kleinstreuer et al. proposed a correlation for particle deposition due to sedimentation and inertial impaction in a G6–G9 airway [5], i.e.,

$$\mathrm{DE} = \left(0.974St^{1.26} + 0.4558\gamma^{0.775} + 13.655St\gamma\right) \times 100\% \quad (9)$$

From the aspect of deposition mechanism, the inertial impaction of the particle is caused by the entrainment of the air. It is reasonable to correlate the DE with the term St^n, i.e., the U^n. However, the deposition caused by particle sedimentation correlates to the sedimentation parameter γ linearly based on the previous discussion and the experiment [39]. Also considering the possible deposition due to the combined effects of sedimentation and impaction, the third term should be $St^n\gamma$. Thus, the deposition efficiency in the G11 to G14 airway can be correlated as

$$\mathrm{DE} = \left(aSt^b + c\gamma + dSt^b\gamma\right) \times 100\% \quad (10)$$

For the simulations of this study ($5.78 \times 10^{-4} < St < 0.226$, $1.54 \times 10^{-4} < \gamma < 0.06$), $a = 3.397$, $b = 1.519$, $c = 10.885$, and $d = -1.284$ yield the best fit (see Fig. 8), where adjusted $R^2 = 0.996$. This result is improved compared to the value of 0.93 obtained by Kleinstreuer et al. [5].

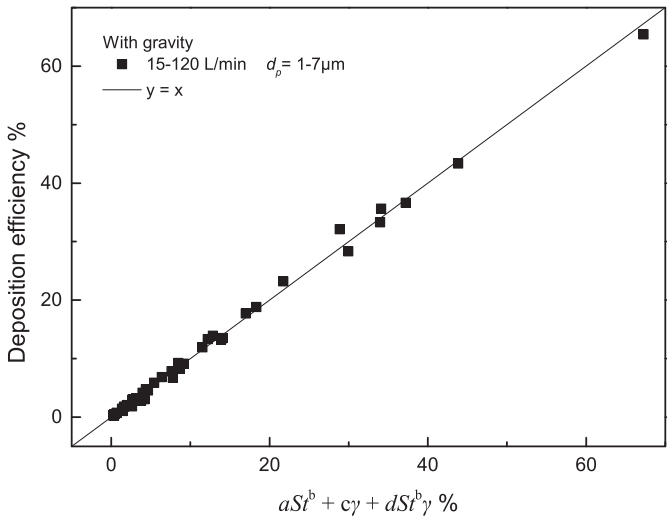

Fig. 8. Prediction of deposition efficiency in the triple bifurcation airway with gravity using the new correlation.

5. Conclusions

Particle deposition due to gravitational sedimentation and inertial impaction in a triple bifurcation airway have been analyzed for particle diameter ranging from 1 μm to 7 μm and inhalation flow rate between 15 and 120 L/min. The airway generations, i.e., G11 to G14, was selected according to the approach of matching Stokes number and sedimentation parameter, which was proposed based on the observation of our previous experimental measurements [39]. The particle deposition patterns and regional deposition efficiencies of simulations with and without gravity have been compared. The following conclusions can be drawn:

(1) In contrast to the upper lung generations, the airflow distributions in the lower generations are almost equal in each daughter tubes.

(2) There are distinct differences in the deposition patterns of 2.5 μm particles under different inhalation flow rates conditions when comparing the simulation results with and without gravity. Particle deposition dominated by gravitational sedimentation is observed.

(3) Particle deposition efficiencies have been analyzed as functions of Stokes number and sedimentation parameter individually. Minimum deposition efficiency is existed for large particles, i.e., 5 μm and 7 μm in diameters when considering gravity. The deposition efficiency decreases with increased Stokes number for small particles, which indicates that the dominant deposition mechanism is sedimentation.

(4) A new correlation function is proposed for predicting particle deposition efficiency when $5.78 \times 10^{-4} < St < 0.226$ and $1.54 \times 10^{-4} < \gamma < 0.06$, i.e.,

$$\mathrm{DE} = \left(3.397St^{1.519} + 10.885\gamma - 1.284St^{1.519}\gamma\right) \times 100\% \quad (11)$$

These deposition characteristics could be utilized for patient-specific pulmonary targeted drug delivery in the lower airway or the alveolar regions. For example, breath-holding or slow inhalation should be adopted for drug targeting the lower lung generations (G11 to G14 in this study) when the drug particle is traveling through these generations. Higher flow rate at the end of inhalation could decrease the deposition due to sedimentation in the lower airway, if the drug particle is designated to deposit in alveolar regions, e.g., the inhaled insulin.

This study is limited to the symmetric-in-plane model for G11 to G14 airway. Future works may focus on the combined effects of gravitational sedimentation and inertial impaction in airway units in wider range of airway generations with asymmetric geometries and out-of-plane bifurcations as well as different inclination angles to improve

the correlation function. Furthermore, the effects of the sedimentation and impaction on macroscopic scale could be evaluated, if the improved correlation function can be used with statistics of the airway number, size and inclination angle for different generations.

Acknowledgements

The authors gratefully acknowledge the financial support of the National Natural Science Foundation of China (grant No. 51176035 and No. 51606041), National Natural Science Foundation of Jiangsu Prov. (grant No. BK20160688) and the Scientific Research Subject of Environmental Protection in Jiangsu Province (grant No. 2015018). The Fundamental Research Funds for the Central Universities are also acknowledged.

References

[1] C. Kleinstreuer, Z. Zhang, J. Donohue, Targeted drug-aerosol delivery in the human respiratory system, Annu. Rev. Biomed. Eng. 10 (2008) 195–220.
[2] Y. Zhang, T.L. Chia, W.H. Finlay, Experimental measurement and numerical study of particle deposition in highly idealized mouth-throat models, Aerosol Sci. Technol. 40 (2006) 361–372.
[3] Y. Zhang, W.H. Finlay, E.A. Matida, Particle deposition measurements and numerical simulation in a highly idealized mouth–throat, J. Aerosol Sci. 35 (2004) 789–803.
[4] Z. Zhang, C. Kleinstreuer, C. Kim, Gas–solid two-phase flow in a triple bifurcation lung airway model, Int. J. Multiphase Flow 28 (2002) 1021–1046.
[5] C. Kleinstreuer, Z. Zhang, C.S. Kim, Combined inertial and gravitational deposition of microparticles in small model airways of a human respiratory system, J. Aerosol Sci. 38 (2007) 1047–1061.
[6] S. Chhabra, A.K. Prasad, Flow and particle dispersion in a pulmonary alveolus—part ii: effect of gravity on particle transport, J. Biomech. Eng. 132 (2010), 051010. .
[7] Y.-S. Cheng, Y. Yamada, H.-C. Yeh, D.L. Swift, Diffusional deposition of ultrafine aerosols in a human nasal cast, J. Aerosol Sci. 19 (1988) 741–751.
[8] P. Zamankhan, G. Ahmadi, Z. Wang, P.K. Hopke, Y.-S. Cheng, W.C. Su, D. Leonard, Airflow and deposition of nano-particles in a human nasal cavity, Aerosol Sci. Technol. 40 (2006) 463–476.
[9] P.F. Ghalati, E. Keshavarzian, O. Abouali, A. Faramarzi, J. Tu, A. Shakibafard, Numerical analysis of micro-and nano-particle deposition in a realistic human upper airway, Comput. Biol. Med. 42 (2012) 39–49.
[10] C.S. Kim, D.M. Fisher, Deposition characteristics of aerosol particles in sequentially bifurcating airway models, Aerosol Sci. Technol. 31 (1999) 198–220.
[11] C.S. Kim, D.M. Fisher, D.J. Lutz, T.R. Gerrity, Particle deposition in bifurcating airway models with varying airway geometry, J. Aerosol Sci. 25 (1994) 567–581.
[12] Y. Zhou, Y.-S. Cheng, Particle deposition in a cast of human tracheobronchial airways, Aerosol Sci. Technol. 39 (2005) 492–500.
[13] T. Sera, K. Uesugi, N. Yagi, H. Yokota, Numerical simulation of airflow and microparticle deposition in a synchrotron micro-CT-based pulmonary acinus model, Comput. Methods Biomech. Biomed. Engin. 18 (2015) 1427–1435.
[14] Y.S. Cheng, Y. Zhou, W.-C. Su, deposition of particles in human mouth–throat replicas and a USP induction port, J. Aerosol Med. Pulm. Drug Deliv. 27 (2014) 1–9.
[15] K. Inthavong, J. Tu, C. Heschl, Micron particle deposition in the nasal cavity using the v2–f model, Comput. Fluids 51 (2011) 184–188.
[16] Z. Zhang, C. Kleinstreuer, C.S. Kim, Effects of curved inlet tubes on air flow and particle deposition in bifurcating lung models, J. Biomech. 34 (2001) 659–669.
[17] I. Balásházy, T.B. Martonen, W. Hofmann, Simultaneous sedimentation and impaction of aerosols in two-dimensional channel bends, Aerosol Sci. Technol. 13 (1990) 20–34.
[18] T.R. Gerrity, P.S. Lee, F.J. Hass, A. Marinelli, P. Werner, R. Lourenco, Calculated deposition of inhaled particles in the airway generations of normal subjects, J. Appl. Physiol. 47 (1979) 867–873.
[19] L. Augusto, J. Gonçalves, G. Lopes, CFD Evaluation of the Influence of Physical Mechanisms, Particle Size, and Breathing Condition on the Deposition of Particulates in a Triple Bifurcation Airway, Water, Air, & Soil Pollution, 227, 2016 56.
[20] L. Augusto, G. Lopes, J. Gonçalves, A CFD study of deposition of pharmaceutical aerosols under different respiratory conditions, Braz. J. Chem. Eng. 33 (2016) 549–558.
[21] Y. Liu, E.A. Matida, M.R. Johnson, Experimental measurements and computational modeling of aerosol deposition in the Carleton-civic standardized human nasal cavity, J. Aerosol Sci. 41 (2010) 569–586.
[22] P.W. Longest, S. Vinchurkar, Effects of mesh style and grid convergence on particle deposition in bifurcating airway models with comparisons to experimental data, Med. Eng. Phys. 29 (2007) 350–366.
[23] G. Tian, P.W. Longest, G. Su, R.L. Walenga, M. Hindle, Development of a stochastic individual path (SIP) model for predicting the tracheobronchial deposition of pharmaceutical aerosols: effects of transient inhalation and sampling the airways, J. Aerosol Sci. 42 (2011) 781–799.
[24] X. Chen, W. Zhong, B. Sun, B. Jin, X. Zhou, Study on gas/solid flow in an obstructed pulmonary airway with transient flow based on CFD–DPM approach, Powder Technol. 217 (2012) 252–260.
[25] X. Chen, W. Zhong, X. Zhou, B. Jin, B. Sun, CFD–DEM simulation of particle transport and deposition in pulmonary airway, Powder Technol. 228 (2012) 309–318.
[26] L. Golshahi, G. Tian, M. Azimi, Y.-J. Son, R. Walenga, P.W. Longest, M. Hindle, The use of condensational growth methods for efficient drug delivery to the lungs during noninvasive ventilation high flow therapy, Pharm. Res. 30 (2013) 2917–2930.
[27] Á. Farkas, I. Balásházy, Quantification of particle deposition in asymmetrical tracheobronchial model geometry, Comput. Biol. Med. 38 (2008) 508–518.
[28] B. Asgharian, S. Anjilvel, Inertial and gravitational deposition of particles in a square cross section bifurcating airway, Aerosol Sci. Technol. 20 (1994) 177–193.
[29] I. Balásházy, T.B. Martonen, W. Hofmann, Inertial impaction and gravitational deposition of aerosols in curved tubes and airway bifurcations, Aerosol Sci. Technol. 13 (1990) 308–321.
[30] J. Sznitman, T. Heimsch, J.H. Wildhaber, A. Tsuda, T. RÃ]sgen, Respiratory flow phenomena and gravitational deposition in a three-dimensional space-filling model of the pulmonary acinar tree, J. Biomech. Eng. 131 (2009), 031010. .
[31] B. Asgharian, W. Hofmann, R. Bergmann, Particle deposition in a multiple-path model of the human lung, Aerosol Sci. Technol. 34 (2001) 332–339.
[32] C. Kleinstreuer, Z. Zhang, Optimal drug-aerosol delivery to predetermined lung sites, J. Heat Transf. 133 (2011), 011002. .
[33] C. Kleinstreuer, Z. Zhang, Targeted drug aeroso deposition analysis for a four-generation lung airway model with hemispherical tumors, J. Biomech. Eng. 125 (2003) 197–206.
[34] H. Luo, Y. Liu, X. Yang, Particle deposition in obstructed airways, J. Biomech. 40 (2007) 3096–3104.
[35] W. Hofmann, I. Balásházy, L. Koblinger, The effect of gravity on particle deposition patterns in bronchial airway bifurcations, J. Aerosol Sci. 26 (1995) 1161–1168.
[36] B. Ma, V. Ruwet, P. Corieri, R. Theunissen, M. Riethmuller, C. Darquenne, CFD simulation and experimental validation of fluid flow and particle transport in a model of alveolated airways, J. Aerosol Sci. 40 (2009) 403–414.
[37] B. Ma, C. Darquenne, Aerosol deposition characteristics in distal acinar airways under cyclic breathing conditions, J. Appl. Physiol. 110 (2011) 1271–1282.
[38] M.C. Piglione, D. Fontana, M. Vanni, Simulation of particle deposition in human central airways, Eur. J. Mech. B. Fluids 31 (2012) 91–101.
[39] X. Chen, W. Zhong, J. Tom, C. Kleinstreuer, Y. Feng, X. He, Experimental-computational study of fibrous particle transport and deposition in a bifurcating lung model, Particuology 28 (2016) 102–113.
[40] Z. Zhang, C. Kleinstreuer, C. Kim, Flow structure and particle transport in a triple bifurcation airway model, J. Fluids Eng. 123 (2001) 320–330.
[41] Z. Zhang, C. Kleinstreuer, C.S. Kim, Comparison of analytical and CFD models with regard to micron particle deposition in a human 16-generation tracheobronchial airway model, J. Aerosol Sci. 40 (2009) 16–28.
[42] S. Morsi, A. Alexander, An investigation of particle trajectories in two-phase flow systems, J. Fluid Mech. 55 (1972) 193–208.
[43] E.R. Weibel, Morphometry of the human lung, Academic Press, New York, 1963.
[44] Fluent 14.5 Users Guide. , ANSYS Inc., Canonsburg, PA, USA, 2012.
[45] Z. Zhang, C. Kleinstreuer, C. Kim, Cyclic micron-size particle inhalation and deposition in a triple bifurcation lung airway model, J. Aerosol Sci. 33 (2002) 257–281.
[46] B. Grgic, W. Finlay, A. Heenan, Regional aerosol deposition and flow measurements in an idealized mouth and throat, J. Aerosol Sci. 35 (2004) 21–32.
[47] Y. Liu, E.A. Matida, J. Gu, M.R. Johnson, Numerical simulation of aerosol deposition in a 3-D human nasal cavity using RANS, RANS/EIM, and LES, J. Aerosol Sci. 38 (2007) 683–700.
[48] X. Li, K. Inthavong, J. Tu, Particle inhalation and deposition in a human nasal cavity from the external surrounding environment, Build. Environ. 47 (2012) 32–39.
[49] K. Inthavong, J. Wen, Z. Tian, J. Tu, Numerical study of fibre deposition in a human nasal cavity, J. Aerosol Sci. 39 (2008) 253–265.